Biodegradation (2011) 22:877–896
DOI 10.1007/s10532-010-9445-x

ORIGINAL PAPER

Dimensionless parameters to summarize the influence of microbial growth and inhibition on the bioremediation of groundwater contaminants

M. Mohamed · K. Hatfield

Received: 10 December 2009 / Accepted: 10 December 2010 / Published online: 23 December 2010

Abstract Monod expressions are preferred over zero- and first-order decay expressions in modeling contaminants biotransformation in groundwater because they better represent complex conditions. However, the wide-range of values reported for Monod parameters suggests each case-study is unique. Such uniqueness restricts the usefulness of modeling, complicates an interpretation of natural attenuation and limits the utility of a bioattenuation assessment to a small number of similar cases. In this paper, four Monod-based dimensionless parameters are developed that summarize the effects of microbial growth and inhibition on groundwater contaminants. The four parameters represent the normalized effective microbial growth rate (η), the normalized critical contaminant/substrate concentration (S*), the critical contaminant/substrate inhibition factor (N), and the bioremediation efficacy (η*). These parameters enable contaminated site managers to assess natural attenuation or augmented bioremediation at multiple sites and then draw comparisons between disparate remediation activities, sites and target contaminants. Simulations results are presented that reveal the sensitivity of these dimensionless parameters to Monod parameters and varying electron donor/acceptor loads. These simulations also show the efficacy of attenuation (η*) varying over space and time. Results suggest electron donor/acceptor amendments maintained at relative concentrations S* between 0.5 and 1.5 produce the highest remediation efficiencies. Implementation of the developed parameters in a case study proves their usefulness.

Keywords Modeling · Bioremediation · Monod kinetics · Inhibition · Dimensionless · Groundwater

M. Mohamed (✉)
Civil and Environmental Engineering Department, United Arab Emirates University, P.O. Box 17555, Al-Ain, UAE
e-mail: m.mohamed@uaeu.ac.ae

M. Mohamed
Irrigation and Hydraulics Department,
Faculty of Engineering, Cairo University,
P.O. Box 12211, Giza, Egypt

K. Hatfield
Civil and Coastal Engineering Department,
University of Florida, P.O. Box 116580, Gainesville,
FL 32611, USA

Introduction

Modeling contaminant biodegradation is an essential element of subsurface bioremediation design and risk assessment. Several models that simulate subsurface contaminant attenuation have been developed varying from those with first-order decay coefficients to others using Monod expressions (e.g. Tomson and Jackson 2000; Murphy and Ginn 2000; Murphy et al. 1997; Brun and Engesgaard 2002; Prommer et al. 2002). Alvarez-Cohen and Speitel (2001) reviewed the cometabolism kinetics for chlorinated solvents.

Murphy and Ginn (2000) presented an overview of approaches used to represent physicochemical and biological processes in porous media. They categorized the processes that control subsurface contaminants biodegradation into physicochemical and biological processes. The physicochemical processes include advection, diffusion, dispersion, exclusion, straining, and physical filtration. The physicochemical processes are primarily based on the structure and properties of the groundwater flow system and porous media. Consequently, most reactive transport models incorporate some of the major physical processes, and these processes have been the focus of numerous experimental and numerical modeling studies on colloid and bio-colloid research.

Molz et al. (1986) separate biological process modeling into three distinct conceptual approaches. The first assumes unconsolidated solid aquifer materials are uniformly covered by a thin biofilm (e.g. Rittmann et al. 1980; Bouwer and McCarty 1984; Bouwer and Cobb 1987; Champagne et al. 1999; Långmark et al. 2004; Kim et al. 2004; Iliuta and Larachi 2005; Liang and Chiang 2007; Liang et al. 2007; Simpson 2008; Buchanan et al. 2008). In a second approach, bacteria are assumed to grow and attenuate contaminants within small discrete colonies (or 'micro-colonies') attached to surfaces of aquifer materials (e.g. Watson and Gardner 1986; Yoshida et al. 2006). Both biofilm and micro-colony assume substrate (i.e. contaminant) reaction kinetics are either first-order, instantaneous reaction, or multi-term Monod (Monod 1949). Other investigators (e.g. Bazin et al. 1976; Corapcioglu and Haridas 1984, 1985; Borden and Bedient 1986; Celia and Kindred 1987; Champagne et al. 1999; Långmark et al. 2004; Kim et al. 2004; Iliuta and Larachi 2005; Mohamed et al. 2006; Bauer et al. 2008) adopted a third approach which assumes partitioning between free flowing and adsorbed microorganisms (Corapcioglu and Haridas 1984, 1985) but their distribution and interaction play no role in depicting the growth dynamics (Baveye and Valocchi 1989). Monod expressions are typically assumed for most applications of this approach, because knowledge of the microorganism population distribution within the pore space is not required (Odencrantz et al. 1990). Regardless of the modeling approach taken, one of the challenges is obtaining reliable kinetic parameters to simulate in situ biotransformations.

Few studies (e.g. Clement et al. 2000; Schirmer et al. 2000) have used reactive transport models to evaluate how biodegradation processes and rates change from the laboratory to the field, which is critical information for field-scale remediation design. Clement et al. (2000) used multispecies reactive transport modeling to understand processes and rates that control natural attenuation at the Dover Air Force Base site in Delaware. Their calibrated two-dimensional model predicted the observed distributions of TCE, PCE, DCE, vinyl chloride (VC), and chloride plumes. The field-scale decay rates were within the range of values that were estimated based on laboratory-scale microcosm and field-scale transect analyses. Phanikumar et al. (2005) developed a three-dimensional reactive transport model of carbon tetrachloride (CT) bioremediation at the Schoolcraft site in western Michigan. The model simulates the transport and reactions of aqueous and sorbed phase CT, acetate, and electron acceptor (nitrate). The model was used to predict solute concentrations across the site using laboratory-based reaction parameters. A reasonable agreement was found between predicted and observed acetate and nitrate concentrations. Schirmer et al. (1999) used the numerical model BIOBATCH to determine Monod kinetic parameters for laboratory batch experiments. They indicated that measurements of several initial substrate concentrations were crucial to overcome the problem of non-uniqueness of the fitted Monod parameters. Their calculated Monod parameters for the batch degradation experiments were reasonable and comparable to other literature values. Schirmer et al. (2000) used the numerical model BIO3D and applied laboratory-derived Monod kinetic degradation parameters to simulate dissolved gasoline transport and degradation at the Canadian Forces Base site, Borden. Tebes-Stevens and Valocchi (2000) developed approaches to compute reaction parameter sensitivity coefficients to gain insight into the relative significance of parameters and to rank them in terms of their importance. Schafer (2001) applied the 3-D numerical reactive transport model TBC to understand contaminant spread and pump and treat remediation of xylene at an abandoned refinery site in Germany. Mayer et al. (2001) used multicomponent reactive transport modeling to evaluate the potential for natural attenuation of a plume containing phenolic compounds at a site in West Midlands, UK. Phanikumar et al. (2002) developed a seven-component reactive transport model to

describe microbially mediated CT degradation. It was found that the CT degradation rate in the columns was lower than values obtained from batch studies, and processes in addition to the growth and decay of strain KC cells (due to native flora) are necessary to describe the observed nitrate consumption. Phanikumar and Hyndman (2003) showed that considerations of bioavailability have a profound effect on degradation. Bioattenuation involving organic substrates and redox-sensitive species has also been the focus of several studies (e.g. Prommer et al. 1998; Brooks et al. 1999; Saiers et al. 2000; Vainshtein et al. 2003; Curtis 2003; Khan and Husain 2003; Guha 2004; Yu et al. 2007; Bauer et al. 2008). To model these systems, it is critical to capture the biogeochemistry.

Many of the early models simulated contaminant decay assuming zero order, first order, and instantaneous reaction kinetics. For zero-order reactions, the rate of substrate transformation is assumed independent of concentration (Sims et al. 1989). Zero-order decay is simple and easy to use; however, the fact that it does not consider changes in the substrate concentration limits its applicability in subsurface modeling. First-order reactions are linearly dependent on substrate concentrations. However, it is difficult to estimate field-scale first-order parameters from laboratory and field data, and it is a poor assumption that first-order parameters estimated for one field site are transferable to another (Chapelle and Lovely 1990; Schirmer et al. 1999; Goudar and Strevett 2000). Furthermore, first-order reaction models cannot distinguish between aerobic and anaerobic conditions, nor can they include coupled reaction constraints imposed by ancillary electron donor/acceptors reactions and microbial growth. Instantaneous reactions between electron acceptor/donor and contaminant are employed when microbial growth rates are relatively high compared to the groundwater velocities (Borden et al. 1984; Koussis et al. 2003; Atteia and Guillot 2007). This is not always the case in subsurface environments as some contaminants may be easily degraded while others are recalcitrant. Instantaneous reaction kinetics cannot account for cases of varying degradation rates which limits their utility to highly degradable contaminants. Thus, model simulations of natural attenuation predicated on instantaneous reaction kinetics can under predict concentration distributions.

A multiple-term Monod expression is commonly used when it is unknown which species is rate-limiting (Mohamed and Hatfield 2005; Bauer et al. 2008). An important advantage of Monod reaction terms is their ability to simulate zero-, first-, and mixed-order reaction rates. Models based on the Monod terms are favorable over first-order growth and decay terms primarily because the later predict unbounded growth (or decay) and these are not found in nature. In general, Monod reaction terms describe nonlinear contaminant attenuation processes which are coupled to microbial growth and in turn spatial and temporal variations in microbial biomass (MacQuarrie et al. 1990). Bedient et al. (1994) showed Monod model simulations were more accurate than those derived from instantaneous reactions and first-order kinetics. Bekins et al. (1997) compared results from zero- and first-order models to a Monod model and found that the first-order model invalid for substrate concentrations above the half-saturation constant. Dette et al. (2003) demonstrated theoretically that the application of optimal design theory in Monod model is an efficient method for both parameter value identification and economic use of experimental resources. More recently, Strigula et al. (2009) presented the optimal design method as a computational tool for the efficient design of experiments in the Monod model.

Monod expressions uniquely take into consideration both microbial population and substrate levels, as interactions between these levels greatly affect the pattern of contaminant degradation (Simkins and Alexander 1984). However, the dependency of degradation rates on numerous parameters that take on a broad range of values complicates efforts to use Monod expressions to characterize biodegradation at any given site much less compare results between sites. Previous investigators developed simplified and modified Monod expressions (e.g. Bell and Binning 2002; Ribes et al. 2004; Strigula et al. 2009; McCuen and Surbeck 2008) in order to describe laboratory and field results. Others developed dimensionless parameters to facilitate interpretations and applications of Monod reactions in batch reactors (e.g. Lai and Shieh 1997; Tanyola and Tuncel 1993; Muslu 2000). In this paper, four dimensionless parameters are derived from Monod expressions to facilitate the application, description, and interpretation of Monod-based contaminant biodegradation in groundwater as influenced by microbial growth and inhibition. The dimensionless nature of these parameters enables one to compare contaminant attenuation conditions between sites.

Governing equations

In this paper, the term substrate is used interchangeably with contaminant; although, it is possible an inhibiting substrate is not a contaminant, but an amendment (i.e. a critical electron donor/acceptor) required to bring about contaminant degradation or transformation (e.g. reduction or oxidation). For a heterogeneous porous medium, the time-dependent reaction–advection–dispersion equation of a contaminant (k) (and/or electron donor/acceptor) whose spatial concentration distribution is denoted by $C(x_i, t)$ is given by:

$$R_k\frac{\partial C_k}{\partial t} = \frac{\partial}{\partial x_i}\left(D\frac{\partial C_k}{\partial x_i}\right) - V\frac{\partial C_k}{\partial x_i} + Q_k^{bio} \quad (1)$$

where x_i is the distance in i direction (i = 1,2,3 or x_i = x, y, z) [L], the local pore water velocity is V [L T^{-1}]; **D** [L^2 T^{-1}] is the tensor of the hydrodynamic dispersion coefficient, and R is the retardation factor [dimensionless]. These equations are coupled through contaminant source/sink terms Q [ML^{-3} T^{-1}] as follows:

$$Q_k^{bio} = \frac{-M\chi_k}{\theta} \quad (2)$$

where M is the microbial biomass concentration [ML^{-3}], θ is the aquifer porosity [dimensionless], and χ_k is the utilization rate of substrate k by the bacterial species (or effective consortium) [T^{-1}]. Utilization of each substrate k by a bacterial species can be written as:

$$\chi_k = \frac{\mu}{Y_k} \quad (3)$$

where Y_k is the yield coefficient [dimensionless] representing the mass of bacterial species produced per unit mass of substrate k utilized. The specific growth rate of the microbial species utilizing substrate k is described by the Haldane model as follows (Andrews 1968):

$$\mu = \mu_{max}\prod_{k=1}^{k=NS}\left(\frac{S_k}{K_c^k + S_k + \frac{S_k^2}{K_i^k}}\right) \quad (4)$$

where μ_{max} is the microbial maximum specific growth rate constant [T^{-1}], K_c^k is the half saturation coefficient for substrate k [ML^{-3}], and K_i^k is the inhibition coefficient representing the concentration of substrate k that exerts toxic effect on the microbial species [ML^{-3}]. From Eq. 4, it evident μ is always less than μ_{max} as long as substrate inhibition exists.

Different schemes of including inhibition in the growth kinetics model exist in the literature (e.g. Edwards 1970; Luong 1987; Ohtake et al. 1990; Yamamoto et al. 1993; Christ and Abriola 2007; Jia et al. 2007). Andrews' (1968) equation (4) is the most commonly used form of growth kinetic model that includes inhibition (e.g. Jackson and Edwards 1972; Shen and Wang 1994; Sheintuch et al. 1995; Chen and Hao 1996; Surmacz-Gorska et al. 1996; López-Fiuza et al. 2002; Carrera et al. 2004; Papagianni et al. 2007). The mass balance equation for growth and decay of the microbial population can be written as:

$$\frac{dM}{dt} = M(\mu - B) \quad (5)$$

where B is the first order decay rate constant which accounts for cell decay.

Dimensionless parameters

Equations 1–5 show that the biodegradation/transformation of a contaminant or of a substrate k depends on many parameters including μ_{max}, K_c^k, K_i^k, B as well as its concentration S_k. A comparison of natural attenuation or augmented bioremediation from different sites and for different contaminants requires dimensionless Monod-based parameters. The first dimensionless parameter presented represents the ratio of net microbial growth rate at any time and location to a hypothetical maximum microbial growth rate assuming substrate inhibition and cell death are absent.

$$\eta = \prod_{k=1}^{k=NS}\left(\frac{S_k}{K_c^k + S_k + \frac{S_k^2}{K_i^k}}\right) - \frac{B}{\mu_{max}} = \frac{\mu - B}{\mu_{max}} = \frac{1}{M\mu_{max}}\frac{dM}{dt} \quad (6)$$

η is the normalized effective microbial growth rate ($\eta = \omega_{act}/\omega_{max}$); where $\omega_{max} = \mu_{max}\ell/Y_cV$ represents, for a unit flow distance (ℓ), the ratio of the convective transport timescale ℓ/V to the timescale required to degrade/transform a unit mass of

contaminant per unit mass of microbes (Y_C/μ_{max}) in the absence of substrate inhibition and microbial cell death (Mohamed et al. 2006); $\omega_{act} = (\mu - B)\ell/Y_c V$ is the ratio of the convective transport timescale to the timescale required to degrade/transform a unit mass of contaminant per net unit mass of microbes ($Y_C/\eta\mu_{max}$) in presence of substrate inhibition and microbial cell death. Both ω_{act} and ω_{max} are equivalent to a DamKohler number of first kind (Rifai and Bedient 1990; Rashid and Kaluarachchi 1999). For $\omega_{act} \leq 1$, contaminant attenuation may be sensitive to local variations in groundwater velocity. This sensitivity may arises because the characteristic maximum specific growth rate for the microbial population, μ_{max} is small; the normalized effective microbial growth rate, η is small due to low substrate concentrations or small because of substrate inhibition; the yield coefficient, Y_C is large, or groundwater velocities are sufficiently high that time require for attenuation is significantly greater than the average groundwater hydraulic residence time. Because η incorporates multiple Monod kinetic parameters including K_c and K_i as well as solutes' concentrations, it can be used to characterize net effect of contaminant attenuation, microbial growth and inhibition over spatial and temporal scales.

The second dimensionless parameter of interest is S_{cr} or the critical substrate concentration. This variable was defined previously in the wastewater treatment literature for bacterial inhibition in batch reactors as the concentration at which μ peaks (e.g. Grady et al. 1999). As indicate above, the maximum feasible value of μ under substrate inhibition is always less than μ_{max} (Eq. 4) in the presence of substrate inhibition. As μ approaches a maximum in the presences of substrate inhibition, it is also the case that $\eta \rightarrow \eta_{max}$. Again, in the presence of substrate inhibition and cell death η_{max} is always <1; however, it represents the maximum feasible normalized microbial growth rate. The critical contaminant/substrate concentration or the critical concentration S_{cr} for any substrate m (one of the k substrates defined earlier), can be obtained by taking the derivative of η (Eq. 6) with respect to this concentration S_m:

$$S_{cr}^{m} = \sqrt{K_c^m K_i^m} \tag{7}$$

After substituting the definition of critical concentration back into Eq. 6, one obtains the function for η_{max}:

$$\eta_{max} = \frac{S_{cr}^{m}}{S_{cr}^{m} + 2K_c^m} \prod_{k=1}^{k=NS-1} \left(\frac{S_k}{K_c^k + S_k + \frac{S_k^2}{K_i^k}} \right) - \frac{B}{\mu_{max}} \tag{8}$$

where S_{cr}^{m} and K_c^m are the respective critical concentration and half-saturation coefficient for substrate m. Linking S_{cr}^{m} to contaminant transport, means comparing spatial and temporal variations in S_m (contaminant concentration here substrate m) to S_{cr}^{m}. To facilitate this comparison, a second dimensionless parameter can be defined to express normalized critical contaminant or substrate concentrations:

$$S^* = \frac{S_m}{S_{cr}^{m}} \tag{9}$$

Substituting this definition back in Eq. 6 gives:

$$\eta(S^*, N) = \frac{S^*}{S^* + \frac{1}{N}(1 + S^{*2})} \prod_{k=1}^{k=NS-1} \frac{S_k}{K_c^k + S_k + \frac{S_k^2}{K_i^k}} - \frac{B}{\mu_{max}} \tag{10}$$

where

$$N = \sqrt{\frac{K_i^m}{K_c^m}} \tag{11}$$

N is yet another dimensionless parameter representing the inhibition factor for contaminant/substrate m. Grady et al. (1999) used the inverse of N to indicate that inhibition in batch reactors is not solely explained by K_i. The appearance of N in Eq. 10 assures inhibition is considered through the relative value of K_i/K_c. Clearly, as N increases or K_i^m increases with respect to K_r^m, and inhibition becomes less important. N will vary between sites and between contaminants; however, the interpretation and the utility of N remain fixed. Thus, S* varies over space and time as contaminant concentrations vary due to advection, dispersion, and microbial biodegradation/transformation; the latter which can be characterized in terms of dimensionless parameters η, N and S_{cr}.

It is generally assumed microbial growth (and in turn contaminant attenuation) is limited by one substrate at any point in time (Grady et al. 1999). Assuming contaminant attenuation and microbial growth are coupled to multiple auxiliary electron donors/acceptors

and nutrients, then inhibition will vary in space and time. These variations are not just due to single substrate concentration variations, it also possible the cause of inhibition transitions between different controlling substrates. However, if inhibition from a single substrate is considered, a family of η curves can be derived for given values of N and B/μ_{max}. Values of B are typically much smaller than μ_{max} (e.g. Schafer 2001; Brusseau et al. 1999) such that B is ignored or assumed zero (e.g. Salvage and Yeh 1997; Wang and Shen 1997; Schirmer et al. 1999, 2000). The same assumption is made here, and the term B/μ_{max} is dropped in Eq. 10. This simplification produces Fig. 1a, a contour plot (on a Log-scale) of η with respect to S* and N. This figure depicts the symmetric behavior of bioremediation potential with respect to Log S*. Similar figures can be generated for values of $B/\mu_{max} > 0$. These figures would look similar to Fig. 1a except with different values reflecting the effect of higher decay rate. Figure 1a suggests the maximum normalized effective microbial growth rate, η_{max} occurs when Log S* is zero (i.e. $S_m = S_{cr}^m$); however, closer examination of Eq. 10 also indicates $\eta \to 1$ if Log S* approaches zero and Log N approaches ∞ (the case where inhibition is negligible or nonexistent). Thus, η_{max} is generally <1, unless the inhibition coefficient K_i is much larger than the half saturation coefficient K_c. For a large range of S* and N values, Fig. 1a can be used to estimate values of η within a plume regardless of location or contaminant type. However, for small changes in S*, Fig. 1b may be more suitable, as it presents a family of η–S* curves for different values of N. In contrast with Fig. 1a, Fig. 1b depicts a non-symmetric behavior of η with respect to S*. That is, η increases with S* and arrives at the maximum feasible value (η_{max}) for S* equal to 1.0 ($S_m = S_{cr}^m$), and then it decreases at a rate dependent on the value of N. Together the contaminant, auxiliary electron acceptors/donors, and the microbial consortium define the value of N and in turn the upper limit on the remediation potential η_{max}.

Using the definition of N in Eq. 8, the following expression can be derived for the maximum feasible normalized microbial growth rate:

$$\eta_{max} = \frac{N}{N+2} \prod_{k=1}^{k=NS-1} \left(\frac{S_k}{K_c^k + S_k + \frac{S_k^2}{K_i^k}} \right) \quad (12)$$

The asymmetric curve in Fig. 2 represents the behavior of η_{max} with a change in Log N. This curve is asymmetric around Log N = 0.301 which is equivalent to N = 2 and where $\eta_{max} = 0.5$. At this point, the slope of this curve has a maximum value of 0.576. The asymmetry indicates, for any constant increment of ΔLog N = P about the axis of asymmetry, the following equation is pertinent

$$\frac{10^{\log 2+P}}{10^{\log 2+P}+2} + \frac{10^{\log 2-P}}{10^{\log 2-P}+2} = 1 \quad (13)$$

Because Figs. 1a, b, and 2 are dimensionless, they can be used with a variety of microorganisms or consortia and for different electron acceptors/donors. They can be used in remediation system design or remediation system evaluation. In the case of system design, η_{max} is determined first. Conditions maximizing N will yield the largest feasible η but also guarantee the highest degradation rate over a widest distribution of S* (essentially over the greatest spatial extent of plume). Different combinations of available electron acceptors/donors and microorganisms (endemic or introduced) will yield different estimates of η_{max}. Using identified values of K_i and K_c, values of N and S_{cr}^m can be calculated from which desired levels of applied auxiliary substrate concentrations S_o (electron donor/acceptors added to achieve contaminant remediation) can be determined. It would be impractical to design a system that would maintain the maximum remediation potential η_{max} everywhere in the plume at all times. A more practical target, however, is to design a remediation system with S* in the range of (1.0–1.5) (see Fig. 1b). This would guarantee a spatial distribution of microbial growth near the maximum feasible rate η_{max} at most locations in the plume.

For the purpose of remediation system evaluation, K_i and K_c must be known or determined first. From these parameters, N, S_{cr}^m and η_{max} are respectively determined from Eqs. 7, 11, and 12. Field measured values of S_m and S_k can be used to calculate S* and η (using Eqs. 9 and 10 or Fig. 1a) at all monitoring locations within the plume to compare against the calculated value of η_{max}. When local values of η are close to η_{max} remediation rates are close to optimal. However, at this juncture, it may be more effective to introduce a fourth dimensionless parameter, the "bioremediation efficacy" (η*) or the ratio of the normalized effective microbial growth rate to the maximum

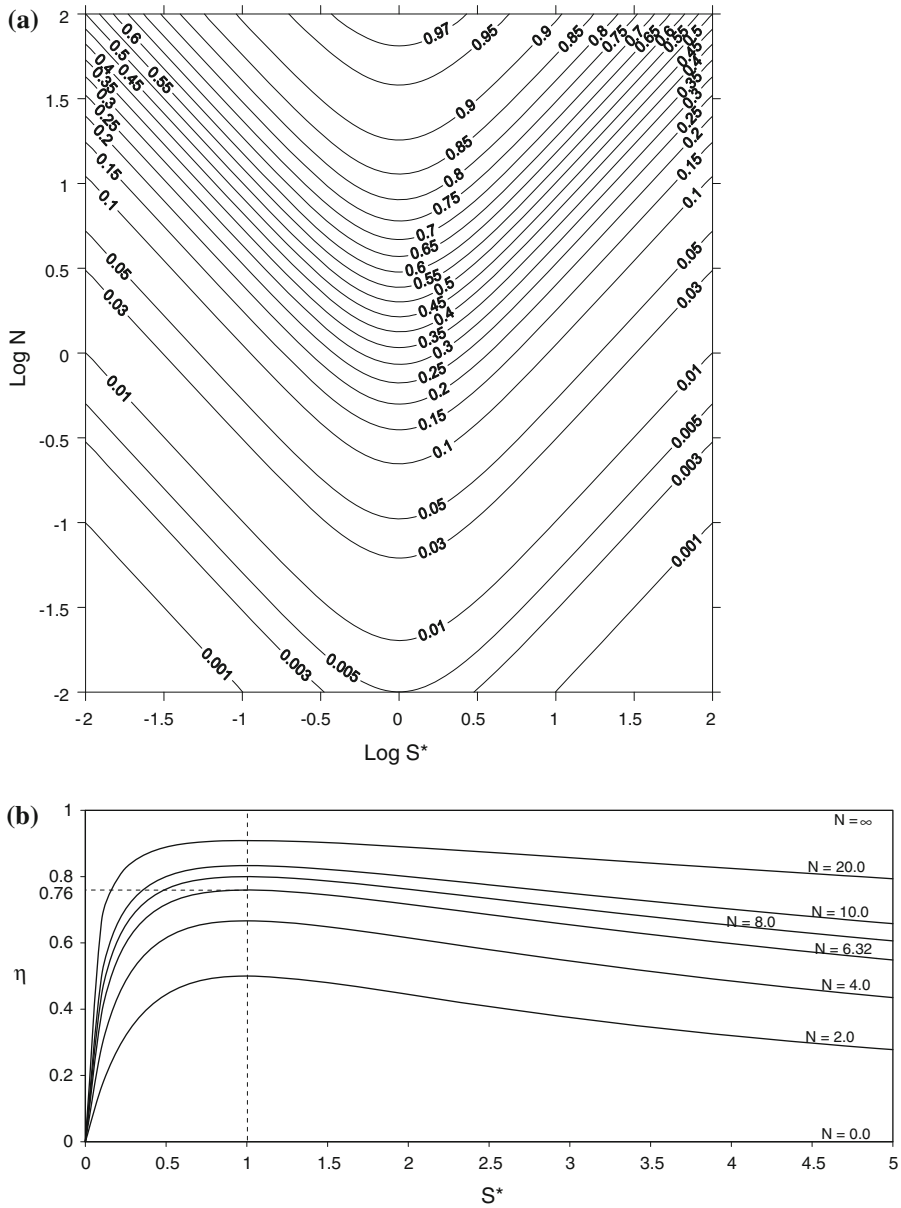

Fig. 1 **a** Contours of normalized effective microbial growth rate (η) in the (N–S*) log domain. **b** Normalized effective microbial growth rate versus critical contaminant/substrate concentration for different values of contaminant/substrate inhibition factor (N)

feasible microbial growth rate. From Eqs. 10 and 12, η^* is defined as follows.

$$\eta^* = \frac{\eta}{\eta_{\max}} = \frac{N + 2}{N + S^* + 1/S^*} \tag{14}$$

The bioremediation efficacy is metric for characterizing bioremediation efficiency. Unlike other previously dimensionless parameters used for bioremediation assessment, η^* is linked to microbial growth, decay and inhibition coefficients (such as μ_{max}, B, K_c, and K_i) as well as availability of both electron donors and acceptors as reflected in S* and S_{cr}. Therefore, this parameter provides a unique description of the actual bioremediation status of an aquifer. Other parameters use traditional mass loss ratios to indicate bioremediation efficiency (such as Phanikumar and Hyndman 2003; Mohamed et al. 2006, 2010a, b, c). This method uses the ratio of biodegraded contaminant mass to the total contaminate mass; whereas η^* (in the same sense) reflects the biodegraded contaminant mass to the total biodegradable contaminant mass. This, in our opinion, presents more accurate estimation of the

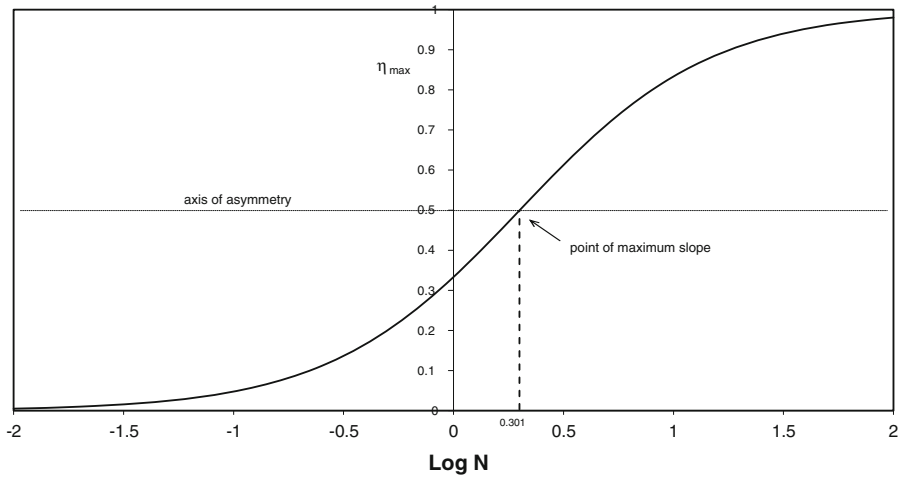

Fig. 2 Change of maximum normalized effective microbial growth rate with Log N

bioremediation potential of the aquifer. For example, $\eta^* = 0.4$ simply states microbial growth and in turn contaminant remediation is occurring at 40% of the feasible maximum and not 40% of μ_{max}. Additionally, the use of bioremediation efficacy is not only useful in the evaluation of natural attenuation or historical remediation activities of contaminated sites, but also helps in the design of feasible bioremediation systems including proper selection of added electron acceptors types and rates. Bioremediation efficacy is particularly valuable, because its determination enables one to assess natural attenuation or augmented bioremediation at any sites and then draw comparisons between disparate remediation activities, sites and target contaminants. Furthermore, the linkage of η^* to the microbial parameters enables one to view η^* in the context of up-scale formulas useful for linking laboratory investigations to field studies.

Figure 3a shows contours of η^* with respect to S* and N on a Log scale. This figure clearly indicates that estimations of η^* is not only site specific, but substrate specific as well. In other words, for the same site, contours of η^* could be developed for each substrate present in the site. This is of particular importance in the cases of cometabolism and competitive inhibition. For example, in the case of cometabolism (Eq. 9 in Table 2, Murphy and Ginn 2000), which involves the transformation of a compound by a microorganism that is incapable of using the compound as a source of energy for growth (e.g. Chang et al. 1993; Criddle 1993; Smith and McCarty 1997), changes in η^* will be solely due to changes in concentrations and not microbial growth. In the case of competitive inhibition (Eq. 8 in Table 2, Murphy and Ginn 2000), when two or microbial species compete for the same nutrients (e.g. Bailey and Ollis 1986; Semprini et al. 1991), estimation of the inhibition constant (K_i), the inhibitor maximum concentration (C_i) and the inhibitor half saturation coefficient (K_c) would be of great importance. These constants are incorporated in the dimensionless parameters N and S* defined in this paper.

Another case that shows the uniqueness of the developed parameters is the case when the biomass M in Eq. 2 is partitioned into attached (M_{im}) and free-swimming (M_m) compartments. In this case Eq. 5 describes the growth of both compartments and can be separated into two equations for M_{im} and M_m (similar to Eqs. 3 and 4 in Table 2, Murphy and Ginn 2000); however, another equation will be needed to describe the transport of the free-swimming microorganisms (M_m) that includes mechanisms of microbial attachment and detachments. Consequently, the concentration of each compartment can be estimated at any time. The values of η (Eq. 6), and thus η^*, can be calculated for each compartment separately or for the total biomass M. This indicates that calculations of η^* could be flexible enough to reflect overall biodegradation or that mediated by each microbial compartment. Thus, the above discussion suggests that contours of η^* are not only substrate specific as indicated above, but also species specific. Even for the same microbial species, η^* is compartment (attached or free-swimming) specific.

Figure 3a shows the relation η^*–Log S* is symmetric (similar to Fig. 1a); and that the axis of

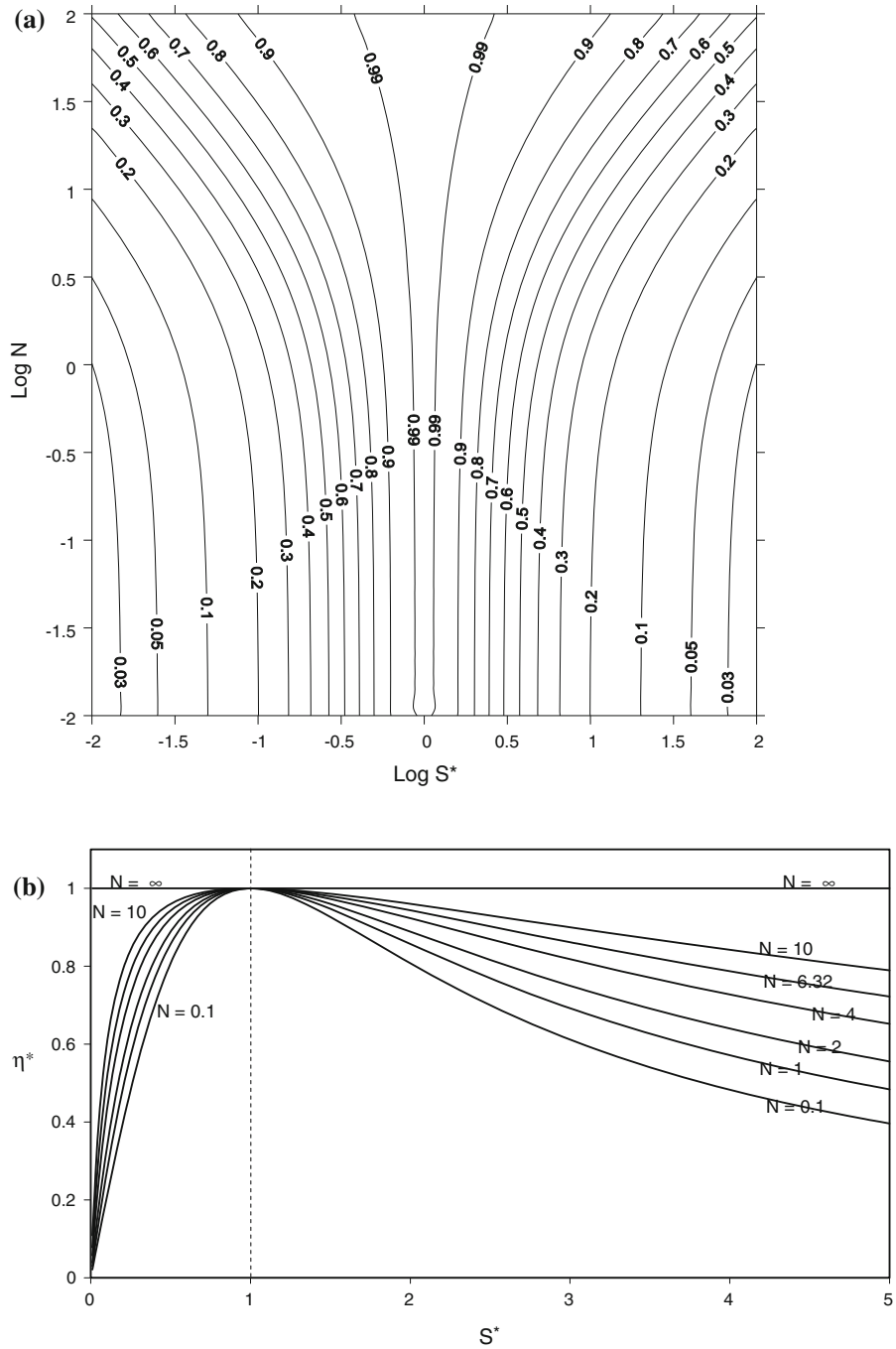

Fig. 3 **a** Contours of bioremediation efficacy (η^*) in the (N–S*) log domain. **b** Bioremediation efficacy (η^*) for different values of the inhibition factor N

symmetry is at Log S* = 0 (i.e. S* = 1). The importance of designing a remediation system or inducing remediation conditions that maximize N is evident in Fig. 3a. η^* contours are shown extending away from the axis of symmetry as the value of N increases, which suggests the highest remediation efficacy can be maintained with less dependence on substrate variations for S* near 1.0. Thus, higher remediation efficacies can be achieved over more of the contaminant plume. For example, if it is assumed that $-2 <$ Log S* < 2 and Log N = 2, the minimum value of η^* obtained is 0.5; this is considerably larger than a value of 0.03 obtained when Log N approaches zero (i.e. $K_c = K_i$).

Figure 3b shows a family of η^*–S* curves for different values of N assuming a range of potential contaminants. While this figure is similar to Fig. 1b, it must be the case that $\eta^* = 1$ (i.e. $\eta = \eta_{max}$) when $S^* = 1$ (i.e. $S_m = S_{cr}$) meaning remediation has achieved maximum efficacy. Figure 3a also demonstrates that in order to obtain the highest efficacy (for the same range of S*), larger values of N are required. For example, increasing N by an order of magnitude (from 1 to 10) increases η^* from 0.8 to 0.95 for S* equals 2.3. Again a well design remediation system would maximize N and in turn generate the greatest spatial distribution of elevated values of η^* within the plume.

Numerical simulations and testing

Problem description

To demonstrate the utility of the above dimensionless parameters, a numerical model METABIOTRANS (Mohamed et al. 2006; Mohamed and Hatfield 2007) was used to conduct simulations of a two-dimensional homogeneous horizontal aquifer with dimensions 50 m × 25 m (Fig. 4) using a mesh of 31,250 rectangular elements (250 × 125) and 31,626 nodes. The uniform pore water velocity in the x-direction (V_x) was 0.5 m/d and the respective longitudinal and transverse dispersivities were 0.1 and 0.05 m. The aquifer porosity was assumed to be 0.3. It was assumed that the aquifer was fully contaminated with a hydrocarbon which serves as an electron donor for microorganisms requiring an electron acceptor for the redox reaction to occur. Normally, contaminant biodegradation would occur at the highest rates at the fringes of the contaminant or electron donor (ED) plume where a sufficient supply of an electron acceptor (EA) exists, whereas the lowest rates of bioattenuation occur within

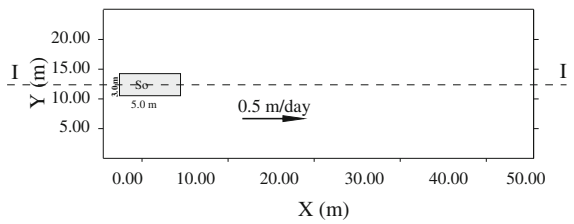

Fig. 4 Problem layout and boundary conditions

Table 1 Input parameters for the different scenarios

Scenario	S_o	K_i	S_{cr}	S_o*	N	η_{max}
1	25	200	31.62	0.79	6.32	0.76
2	50	200	31.62	1.58	6.32	0.76
3	100	200	31.62	3.16	6.32	0.76
4	200	200	31.62	6.32	6.32	0.76
5	100	100	22.36	4.47	4.47	0.69
6	100	50	15.81	6.32	3.16	0.61
7	100	25	11.18	8.94	2.24	0.53

the plume interior or where the supply of requisite EA has been exhausted. The addition of an EA, therefore, is essential to enhance hydrocarbon (ED) bioattenuation within the interior regions of the plume. An electron acceptor such as dissolved nitrate with initial concentration of S_o is supplied to enhance bioremediation as shown in Fig. 4. Table 1 lists assumed values for Monod parameters K_i, and K_c. μ_{max} and Y_c are assumed 0.2 day^{-1} and 0.01, respectively. They kept unchanged in all simulations of this study; and consequently, the value of ω is maintained constant. Therefore, simulated changes in η are due to changes in ω_{act} only. Mohamed et al. (2006) studied the influence of changing ω on contaminants biodegradation in a stochastic framework.

Results and discussion

Several scenarios are simulated to study the spatial and temporal sensitivity of η, η^* and S* to Monod parameters and the concentration of electron acceptor S_o* introduced into the contaminant plume (see Table 1). Results generated using different Monod parameters can be view as results from different contaminants or the same contaminant attenuated under different microbial or site conditions. Simulations and calculated dimensionless parameters are based on representative values for Monod parameter reported in the literature (see Table 2). The first four scenarios examine the sensitivity of η, η^* and S* to S_o*. Constant values are assumed for K_c and K_i which produce fixed values for N and S_{cr} (see Table 1). Scenarios 3, 5, 6, and 7 are used to study the effects of substrate inhibition on spatial and temporal distributions of S* and η^* within the plume.

Figure 5a and b respectively show model simulated remediation potentials η and efficacies η^* along

Table 2 Literature values for some of the biological parameters

Reference	Parameter	Value/range	Calculated dimensionless variables[a]
Papagianni et al. (2007)	μ_{max}	0.23–0.65 h^{-1}	N = 1–7.32
	K_s	0.021–28 mg/l	S_{cr} = 5.6–200
	K_i	0–1500 mg/l	η_{max} = 0.33–0.79
Vavilin and Lokshina (1996)	μ_{max}	0.1–0.585 day^{-1}	N = 1–3.87
	K_s	20–200 mg/l	S_{cr} = 20–245
	K_i	20–300 mg/l	η_{max} = 0.33–0.66
Carrera et al. (2004)	μ_{max}	0.132–0.46 min^{-1}	N = 7.56–26
	K_s	1.7–37 mg/l	S_{cr} = 30.8–107.7
	K_i	559–2908 mg/l	η_{max} = 0.8–0.93
Schafer (2001)	μ_{max}	0.1 day^{-1}	N = 3.8–70.7
	K_s	0.2–70 mg/l	S_{cr} = 14.1–264.6
			η_{max} = 0.66–0.97
Brusseau et al. (1999)	μ_{max}	0.1 day^{-1}	N = 18.3–44.7
	K_s	0.5–3 mg/l	S_{cr} = 22.3–54.8
			η_{max} = 0.9–0.96
Salvage and Yeh (1997)	μ_{max}	0.9288–32.4 day^{-1}	N = 11.5
	K_s	7.5 mg/l	S_{cr} = 86.6
			η_{max} = 0.85
Wang and Shen (1997)	μ_{max}	0.6588–1.5443 day^{-1}	N = 0–13.57
	K_s	5.43–8.64 mg/l	S_{cr} = 0–93
			η_{max} = 0–0.89
Schirmer et al. (1999)	μ_{max}	4.128–4.5 day^{-1}	N = 0–14.6
	K_s	0.79–4.7 mg/l	S_{cr} = 28–68.6
			η_{max} = 0.33–0.79

[a] Calculated based on K_i = 0–1000 mg/l if not given in the corresponding literature

section I–I (see Fig. 4) assuming different initial normalized substrate concentrations (scenarios 1–4). From these figures both η and η^* increase with S_o^* which suggests greater augmented microbial growth and contaminant attenuation occurring over greater portions of the aquifer. S_{cr} is 31.62 mg/l in scenarios 1 through 4; which means maximum microbial growth and bioremediation is achieved when EA concentrations are maintained near 31.62 mg/l. In scenario 3, initial EA concentrations were sufficiently high after 20 days that microbial growth achieved the maximum feasible normalized rate of $\eta_{max} = 0.76$ over much the interior regions of the introduced EA plume. However, when S_o^* is further increased to 6.4, as in scenario 4, it is evident that after 20 days microbial growth is less than η_{max} near the centroid of the EA plume, because elevated EA concentrations are inducing significant inhibition. In fact, because dispersion decreases electron acceptor concentrations between the interior and the fringe regions of the EA plume, remediation potential is seen to rebound and transition through η_{max} on both the leading and trailing sections of the EA plume.

An effective remediation strategy minimizes off-site risks. To achieve this, strategic use of auxiliary substrates (i.e. electron donors/acceptors) is desirable, and the above dimensionless parameters can be used with an available bioremediation simulation model to achieve this goal. Consider again, scenarios 1–4 where at $t = 20$ days a value of $S_o^* = 3.2$ (scenario 3) creates the largest zone of favorable remediation conditions (i.e. maximum remediation potential). Under this scenario, much of the remediation occurs near the source area which reduces risks to receptors close to source area. Using greater concentrations of auxiliary substrates, as in scenario 4, produces residual remediation that is greater than all the other scenarios at 60 days. This strategy may be appropriate

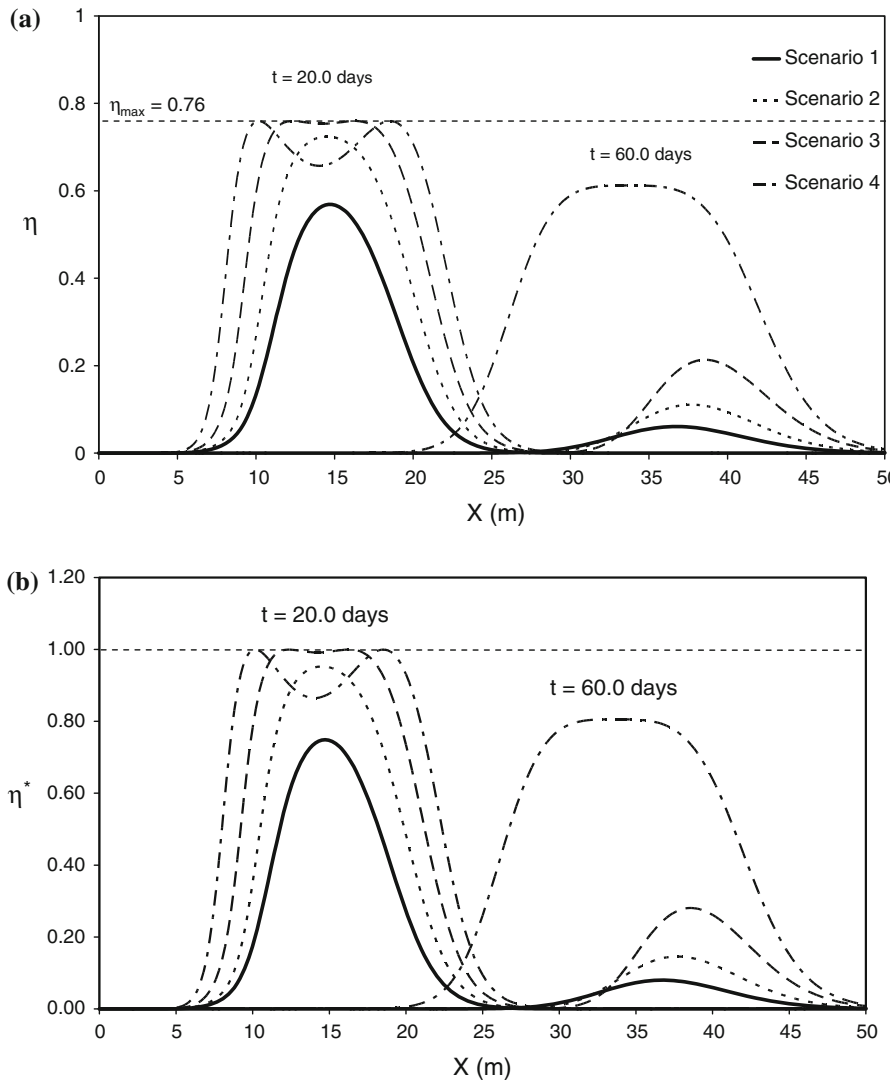

Fig. 5 Effect of changing S_o* on the profile of **a** normalized effective microbial growth rate; **b** bioremediation efficacy, at section I–I for scenarios 1 through 4

where significant residual remediation is needed over greater spatial scales, but off-site risks are low because potential receptors are far from the contaminant source.

Figure 6a illustrates how η varies with respect to N from scenarios 3, 5, 6, and 7. The inhibition factor (N), along with the critical concentration S_{cr}, define the level at which a toxic effects are manifested on microorganisms. As N decreases microorganisms are more vulnerable to inhibition. For example, manifestations of growth inhibition and contaminant attenuation appear less under Scenario 3, because the assumed N is largest. The inhibition factor can portent the likelihood of inhibition; however, the normalized concentration S* provides confirmation. Consider again the third scenario, S* is everywhere less than one after 20 days, and η remains near η_{max}. For smaller values for N, as in scenarios 5, 6 and 7, inhibition is more prevalent; consequently, substrate inhibition constrains microbial growth which in turn produces a trough in the longitudinal spatial profile of η. It follows that smaller values of N produce smaller values of η_{max} (Fig. 2). This leads to larger zones of constrained microbial growth and contaminant degradation/transformation within the electron acceptor plume as shown in Fig. 6a. In addition, decreasing the inhibition factor gives the appearance that EA transport is retarded. Indeed, the EA plume is migrating at a velocity equal to that of groundwater. A reasonable explanation for this 'apparent

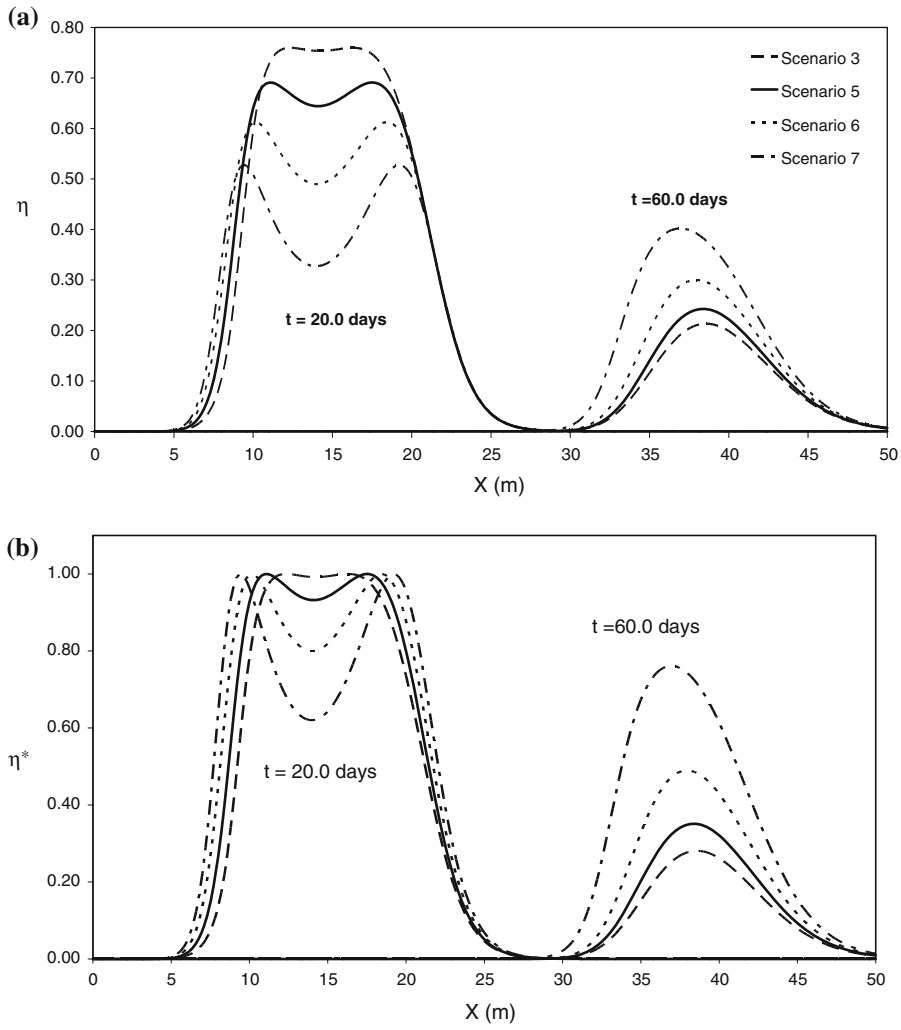

Fig. 6 Effect of changing N on the profile of **a** normalized effective microbial growth rate; **b** bioremediation efficacy, at section I–I for scenarios 3 and 5 through 7

retardation' is that inhibition is limiting EA consumption to the leading edge of the EA plume, which in turn produces an up-gradient shift in the plume centroid (see results for day 60 in Fig. 6a or b). This is happening because inhibition increases rapidly from the leading edge (where EA concentrations are less-than-or-equal to critical, $S^* \leq 1$) to the interior regions of the EA plume (where EA concentrations are much greater than critical, $S^* \gg 1$). The developed dimensionless parameters indicate microbial growth and in turn contaminant attenuation are occurring at a maximum rate in regions where the normalized concentration (S*) is equal to one.

Figure 6b presents longitudinal profiles of the bioremediation efficacy for scenarios 3, 5, 6, and 7. Efficacy is seen to achieve a maximum value of 1 somewhere within the longitudinal η^* profile of each scenario at t = 20 days. However, because introduced EA concentrations were too high in scenarios 5, 6, and 7, contaminant attenuation is depressed within the interior regions of the EA plume as evidenced by efficacies well below 1 and $S^* > 1$. This 'doughnut effect' is clearly illustrated in Fig. 7 for η and η^* and is not evident from contours of S. Areas of significant inhibition are identifiable wherever $S^* > 1$. Predicted contours of bioremediation efficacy (η^*) like those shown in Fig. 7d, can be used to assess the strengths and weaknesses of a proposed remediation designs. The discussion of the following case study shows the implementation of these dimensionless parameters to assess bioremediation in a contaminated site.

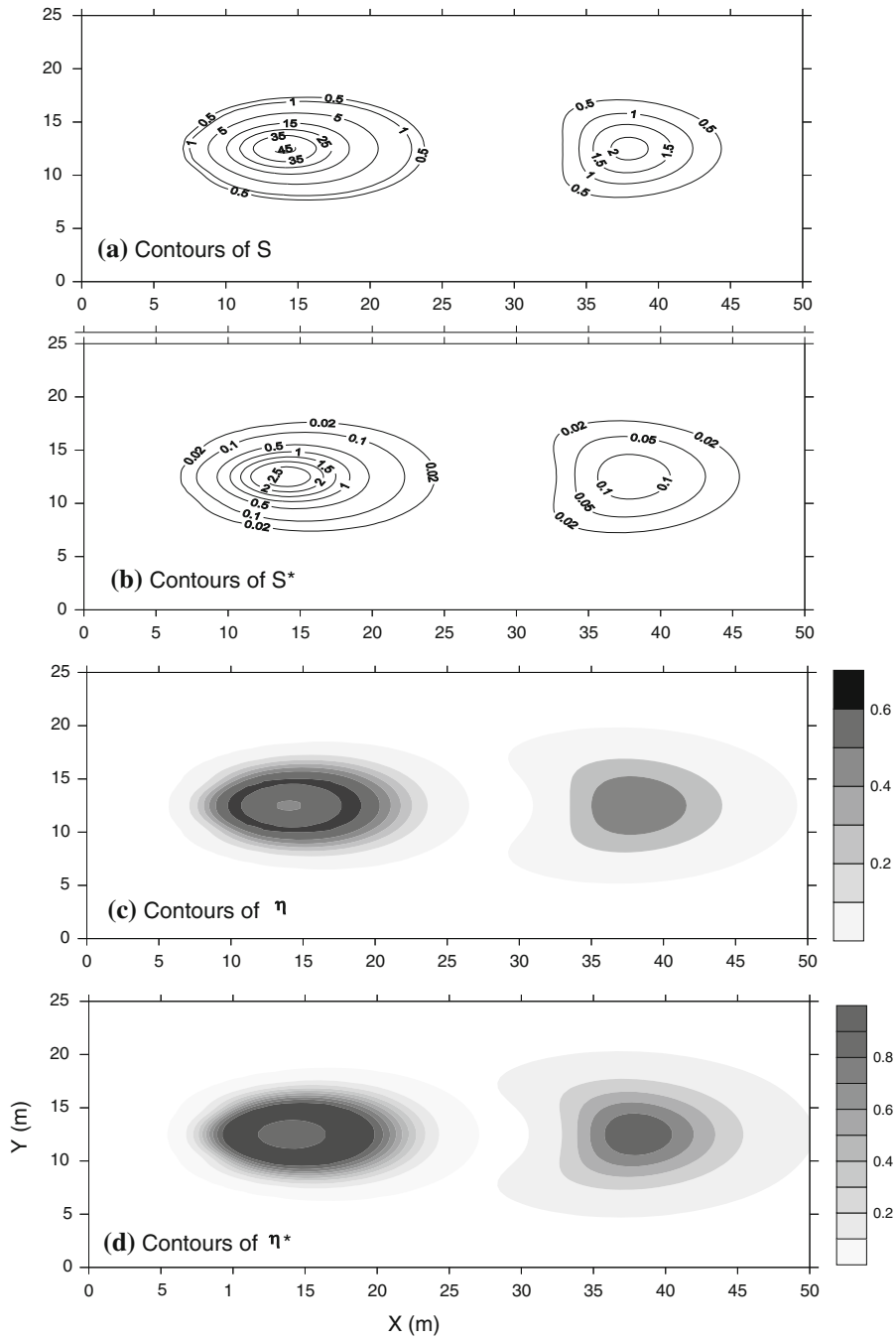

Fig. 7 Contours of **a** EA concentration, **b** relative concentration, **c** normalized effective microbial growth rate, and **d** bioremediation efficacy for scenario 6

Case study: bioremediation of benzene in the contaminated Liwa aquifer, UAE

Dissolved benzene was detected in the shallow unconfined Liwa aquifer, located 150 km southwest of UAE capital Abu Dhabi (Fig. 8). The unconfined Liwa aquifer is the main water supply for irrigation, recreation, and washing for the nearby camp area (Fig. 8) and bottled water is used for drinking. After benzene contamination was discovered in 2000, soil investigations at the site were performed through 142 organic vapor analysis (OVA) readings from 27 test pits field measurements and hydrocarbons were detected in the soil. It was found that contaminated

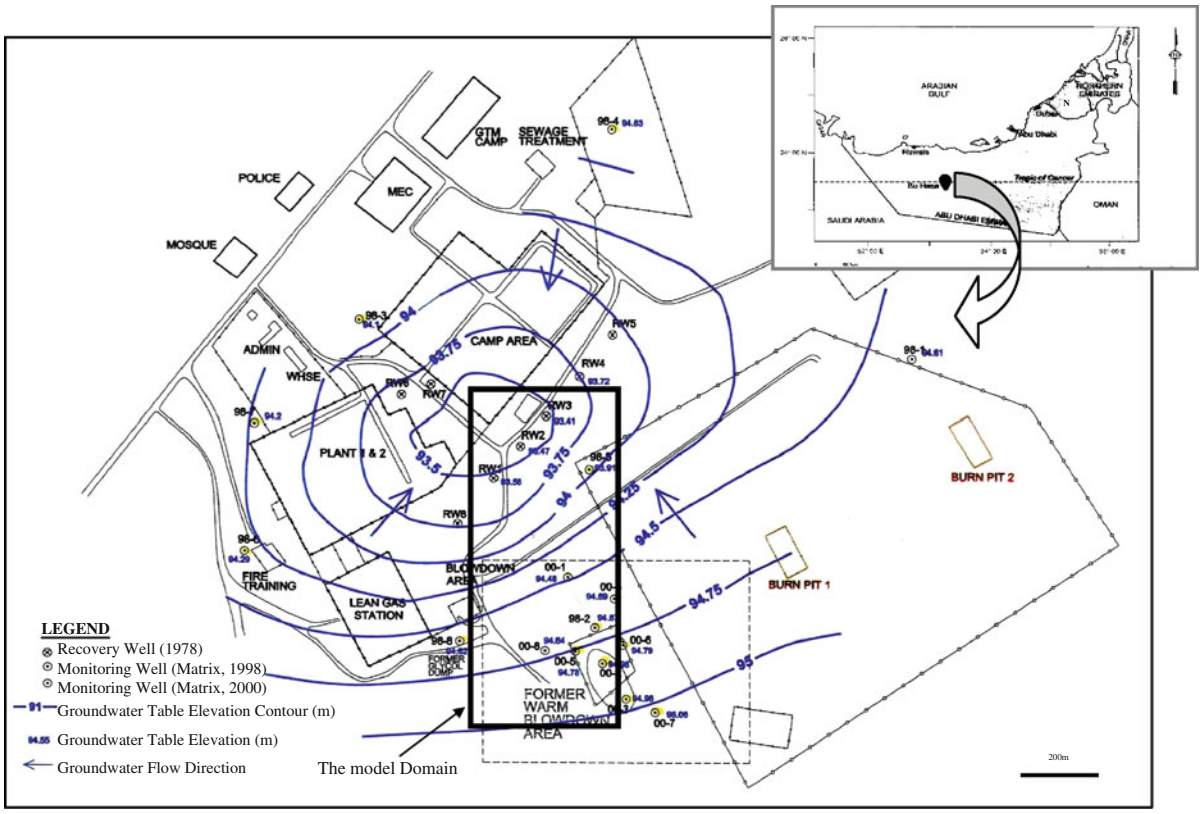

Fig. 8 Site location of Bu Hasa Liquid Recovery Plant, including site plan, water table elevations, and model domain

soil had higher concentrations than background OVA measurements. A monitoring wells network was installed to investigate the extent of hydrocarbon plume from the source zone (Fig. 8). The presence of free phase hydrocarbons floating on the water table was confirmed. The location of the non-aqueous phase liquid (NAPL) measured in the soil is consistent with observations of the dissolved hydrocarbons (Forrest and Arnell 2001). This suggests that the pure NAPL in the soil migrated downward in the unsaturated zone and, being lighter than water, formed a body floating near the water table. For an ideal NAPL mixture in contact with water, the aqueous phase concentration of a component in NAPL can be calculated using the aqueous analog of Raoult's law as the product of its pure aqueous solubility and its mole fraction. Benzene constitutes the highest dissolved concentration of NAPL constituents at the site. Partial dissolution of benzene in the surrounding groundwater results in the formation of a dissolved plume. This dissolved benzene plume migrates by advection and dispersion processes. McNab et al. (1997) assumed that the mole fraction of benzene is equal to 0.5% of its weight fraction, the pure benzene solubility is equal to 1770 mg/l; therefore the aqueous phase concentration of the benzene in NAPL mixture is 8.85 mg/l. However, Johnson et al. (2000) reported that the equilibrium concentration of BETX resulted from typical gasoline mixture in contact with water has a benzene concentration of 18 mg/l. Assuming ideal NAPL mixture, the aqueous phase benzene concentration for this site is estimated to be 8.5 mg/l.

Groundwater elevation data (Woodward 1996) indicate that the regional groundwater flow direction in Liwa aquifer is to the northwest. The hydraulic gradient of the groundwater in the site is variable. The gradient increases towards the pumping wells; therefore, the groundwater velocity also increases in the same area. The hydraulic gradient between the contamination source zone and the supply water wells is 0.25%. Water depths were recorded in November 2000 using the monitoring network and used to calculate groundwater table elevations. Contour map

of groundwater elevation is produced in Fig. 8, based on the records of groundwater levels, and used to estimate groundwater flow direction and horizontal hydraulic gradient. The groundwater flow direction is found to be in agreement with the direction of the regional groundwater flow in Liwa aquifer. Field estimated values for effective porosity of 0.3 and hydraulic conductivity of 1×10^{-4} m/s were used to estimate the average linear groundwater velocity of 25 m/year. It was found that the contamination source is located directly up-gradient of the supply wells; which puts these wells at potential risk of being contaminated.

Simulation of benzene transport in Liwa aquifer is conducted using METABIOTRANS. The simulated model domain covers an area of approximately 292,250 m^2. It was oriented so that it includes the contamination source zone in the southeast corner and the nearest supply wells RW1–RW3 (Fig. 8) representing potential receptors in the northwest corner, directly downstream of the contamination. The domain extends 350 m in x-direction and 850 m in y-direction. A two dimensional finite element grid of 11,900 elements was used for spatial discretization of the study area. Limited measurements were available to determine input parameters for the transport of the dissolved benzene. Values of longitudinal and transverse dispersivities were estimated through model calibration. Model calibration was performed using the observed benzene concentrations at the location of the monitoring well 00-8. Benzene concentration of 0.03 mg/l was observed in this well in July 2000 (Forrest and Arnell 2001). Values of longitudinal and transverse dispersivities were estimated to be 2.3 and 0.23 m, respectively. These values are average for this type of aquifers (e.g. Weaver and Charbeneau 2000).

The calibrated model is used to simulate the transport and fate of the dissolved benzene plume in Liwa aquifer. The slow-release oxygen source (SOS) in situ remediation technique is used in these simulations. This techniques is developed by researchers from the United States Environmental Protection

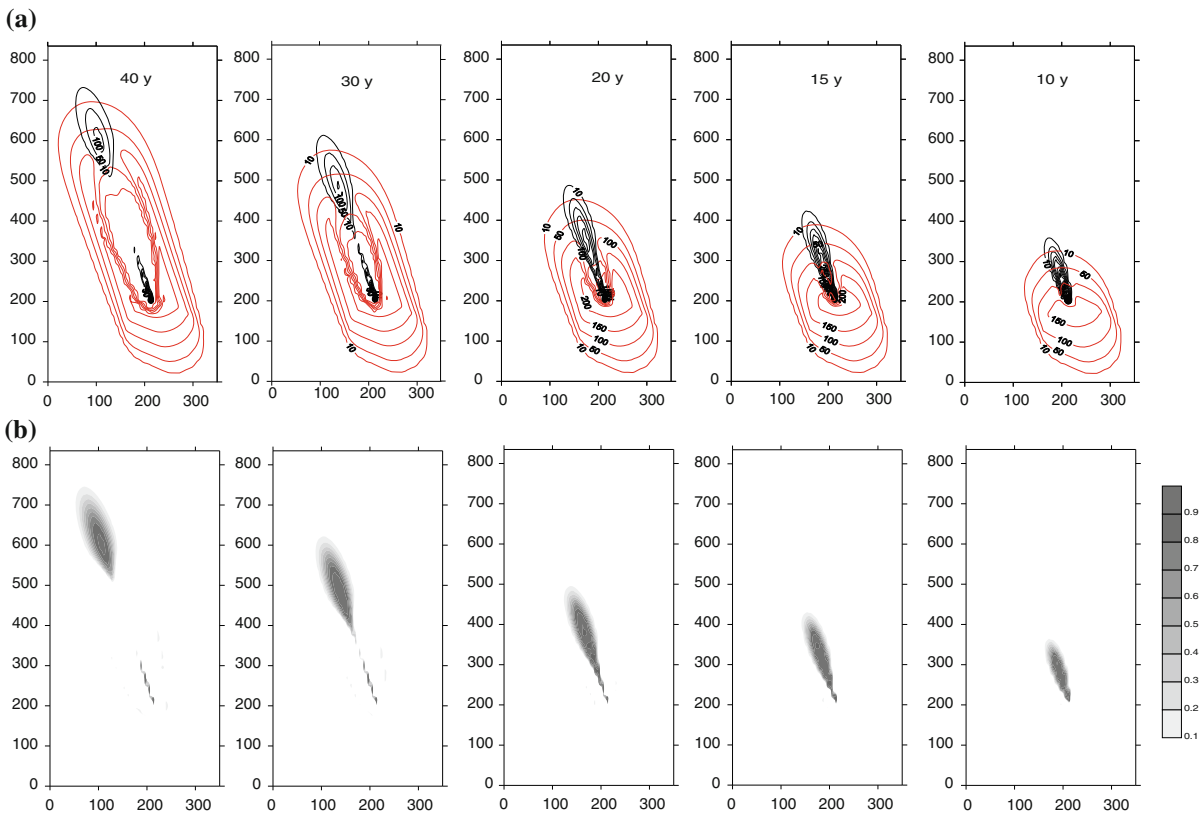

Fig. 9 Evolution of the **a** benzene and oxygen plumes and **b** biodegradation efficacy contours in the aquifer of Bu Hasa field

Agency (US-EPA) in which a constant and controlled release of oxygen through the treatment zone is introduced (Hoover 2007). The technique is based on earlier work of using solid oxygen sources to introduce oxygen in contaminated sites (Vesper et al. 1994). An SOS, located at X = 210 m and Y = 200 m of the domain, is used to enhance bioremediation of the benzene plume. Values of the biological parameters are selected based on values reported in similar studies (e.g. Vavilin and Lokshina 1996; Table 2). The K_s and K_i values are selected to be 125 and 300 mg/l, respectively. Based on these values S_{cr} is calculated to be 194 mg/l and N equals 1.55. Figure 9a shows the two simulated plumes of benzene and oxygen at different times. Using an SOS enhanced remediation in the core of the benzene plume. However, some of the dissolved benzene escaped remediation as depicted by the leading edge of the benzene plume downstream of the injection point. This occurred probably because oxygen concentrations needed time to increase and stimulate bacterial growth and also because microorganisms grow only when the benzene plume encounter the remediation zone. That is why the leading edge of the plume will always encounter lower microbial concentration than the trailing edge, and therefore will continuously experience less bioremediation. Figure 9b shows the evolution of simulated η^* contours. This figure facilitates the assessment of biodegradation efficacy and clearly shows regions of enhanced bioremediation in the aquifer at different times. Simulated concentrations of the oxygen were higher at earlier times (10 and 15 years) than later times which depicts higher values of η^* (near maximum) at earlier times. At later times, because oxygen concentration as well as benzene concentrations decrease due to dispersion and biodegradation, values of η^* decrease as well. However, maximum bioremediation still occurs near the center of the oxygen plume.

Summary and conclusions

This paper presented four dimensionless parameters that enable the evaluation of natural attenuation and augmented bioremediation across different contaminants and sites. These parameters were the normalized effective microbial growth rate (η), the bioremediation efficacy (η^*), the contaminant/substrate inhibition factor (N) and the normalized critical contaminant/substrate concentration (S*). Simulations revealed the sensitivity of these dimensionless parameters to Monod parameters and to varying electron donor/acceptor loads. These simulations also showed the efficacy of attenuation (η^*) varied over space and time. The contaminant/substrate inhibition factor (N) could be used to alert site managers that substrate inhibition could interfere with microbial growth and contaminant attenuation. Whereas the normalized critical contaminant/substrate concentration (S*) would be the most appropriate for confirming the existence and potential whereabouts of inhibition with respect to microbial growth and contaminant attenuations in contaminated aquifers. Results suggested electron donor/acceptor amendments maintained at relative concentrations S* between 0.5 and 1.5 produce the highest remediation efficiencies.

Microorganisms and electron acceptors/donors added to augment remediation should be selected whenever possible to generate a highest substrate inhibition factor (N). This would not only result in higher remediation efficiencies, but would also guarantee higher rates sustained over a wider range of normalized substrate concentrations. Finally, contour maps of bioremediation efficacy (η^*) could be used to provide site-wide characterization of remediation efficiency. The implementation of such contour maps is proven to be useful through the design of a remediation system for a contaminated site using a slow-release oxygen source.

Acknowledgments This research was partially funded by the Environmental Remediation Science Program (ERSP), U.S. Department of Energy: (Grant Number DE-FG02-08ER64585) and the Research Affairs at the UAE University (Grant number 08-01-7-11/09).

References

Alvarez-Cohen L, Speitel GE (2001) Kinetics of aerobic cometabolism of chlorinated solvents. Biodegradation 12(2):105–126

Andrews JF (1968) A mathematical model for the continuous culture of microorganisms utilizing inhibitory substance. Biotechnol Bioeng 10:707–723

Atteia O, Guillot C (2007) Factors controlling BTEX and chlorinated solvents plume length under natural attenuation conditions. J Contam Hydrol 90(1–2):81–104

Bailey JE, Ollis DF (1986) Biochemical engineering fundamentals, 2nd edn. McGraw-Hill, New York

Bauer RD, Maloszewski P, Zhang Y, Meckenstock RU, Griebler C (2008) Mixing-controlled biodegradation in a toluene plume—results from two-dimensional laboratory experiments. J Contam Hydrol 96(1–4):150–168

Baveye P, Valocchi A (1989) An evaluation of mathematical models of the transport of biologically reacting solutes in saturated soils and aquifers. Water Resour Res 25(6): 1413–1421

Bazin MJ, Saunders PT, Prosser JI (1976) Models of microbial interactions in the soil. CRC Crit Rev Microbiol 4: 463–498

Bedient PB, Rifai HS, Newell CJ (1994) Ground water contamination—transport and remediation. Prentice-Hall, Englewood Cliffs, NJ

Bekins BA, Warren E, Godsy ME (1997) Comparing zero- and first-order approximations to the Monod model. In: Proceedings of the fourth international in situ and on-site bioremediation symposium, Battelle Press, New Orleans, LA, vol 5, pp 547–552

Bell LSJ, Binning P (2002) A forward particle tracking Eulerian Lagrangian Localized Adjoint Method for multicomponent reactive transport modelling of biodegradation. Dev Water Sci 47:703–710

Borden RC, Bedient PB (1986) Transport of dissolved hydrocarbons influenced by oxygen-limited biodegradation: 1. Theoretical development. Water Resour Res 22(13): 1973–1982

Borden RC, Lee MD, Wilson JT, Ward CH, Bedient PB (1984) Modeling the migration and biodegradation of hydrocarbons derived from a wood-creosoting process waste. In: Proceedings of the National Water Well Association, American Petroleum Institute conference on petroleum hydrocarbons and organic chemicals in groundwater: prevention, detection and restoration, Houston, TX, pp 130–143

Bouwer EJ, Cobb GD (1987) Modeling of biological processes in the subsurface. Water Sci Technol 19:769–779

Bouwer EJ, McCarty PL (1984) Modeling of trace organics biotransformation in the subsurface. Ground Water 22:433–440

Brooks SC, Carroll SL, Jardine PM (1999) Sustained bacterial reduction of Co(III) EDTA in the presence of competing geochemical oxidation during dynamic flow. Environ Sci Technol 33:3938

Brun A, Engesgaard P (2002) Modelling of transport and biogeochemical processes in pollution plumes: literature review and model development. J Hydrol 256(3–4):211–227

Brusseau M, Xie L, Li L (1999) Biodegradation during contaminant transport in porous media: 1. Mathematical analysis of controlling factors. J Contam Hydrol 37: 269–293

Buchanan W, Roddicka F, Porter N (2008) Removal of VUV pre-treated natural organic matter by biologically activated carbon columns. Water Res 42(13):3335–3342

Carrera J, Jubany I, Carvallo L, Chamy R, Lafuente J (2004) Kinetic models for nitrification inhibition by ammonium and nitrite in a suspended and an immobilised biomass systems. Process Biochem 39(9):1159–1165

Celia MA, Kindred JS (1987) Numerical simulation of subsurface contaminant transport with multiple nutrient biodegradation. In: Proceedings of the international conference on the impact of physiochemistry on the study, design, and optimization of processes in natural porous media, Presses University de Nancy, Nancy, France

Champagne P, Parker WJ, Van-Geel P (1999) Modeling cometabolic biodegradation of organic compounds in biofilms. Water Sci Technol 39(7):147–152

Chang M-K, Voice TC, Criddle CS (1993) Kinetics of competitive inhibition and cometabolism in the biodegradation of benzene, toluene, and p-xylene by two Pseudomonas isolates. Biotechnol Bioeng 41:1057–1065

Chapelle FH, Lovely DR (1990) Rates of bacterial metabolish in deep coastal plain aquifers. Appl Environ Microbiol 56:1865–1874

Chen JM, Hao OJ (1996) Environmental factors and modeling in microbial chromium(VI) reduction. Water Environ Res 68(7):1156

Christ JA, Abriola LM (2007) Modeling metabolic reductive dechlorination in dense non-aqueous phase liquid source-zones. Adv Water Resour 30(6–7):1547–1561

Clement TP, Johnson CD, Sun YW, Klecka GM, Bartlett C (2000) Natural attenuation of chlorinated ethene compounds: model development and field-scale application at the Dover site. J Contam Hydrol 42(2–4):113–140

Corapcioglu MY, Haridas A (1984) Transport and fate of microorganisms in porous media: a theoretical investigation. J Hydrol 72:149–169

Corapcioglu MY, Haridas A (1985) Microbial transport in soils and groundwater: a numerical model. Adv Water Resour 8:188–200

Criddle CS (1993) The kinetics of cometabolism. Biotechnol Bioeng 41:1048–1056

Curtis GP (2003) Comparison of approaches for simulating reactive solute transport involving organic degradation reactions by multiple terminal electron acceptors. Comput Geosci 29:319–329

Dette H, Melas VB, Pepelyshev A, Strigul N (2003) Efficient design of experiments in the Monod model. J R Stat Soc B 65(3):725–742

Edwards VH (1970) The influence of high substrate concentration on microbial kinetics. Biotechnol Bioeng 12: 679–712

Forrest B, Arnell P (2001) Hydrocarbon delineation and pilot testing program at the Bu Hasa Liquids Recovery Plant Abu Dhabi report, United Arab Emirates. Matrix Solutions Inc. Report 01-47

Goudar CT, Strevett KA (2000) Estimating in situ Monod biodegradation parameters using a novel explicit solution of a one-dimensional contaminant transport equation. Ground Water 38:894–898

Grady CPLJ, Daigger GT, Lim HC (1999) Biological wastewater treatment. Marcel Dekker, New York

Guha H (2004) Biogeochemical influence on transport of chromium in manganese sediments: experimental and modeling approaches. J Contam Hydrol 70:1–36

Hoover D (2007) Process for the biodegradation of hydrocarbons and ethers in subsurface soil by introduction of a solid oxygen source by hydraulic fracturing. United States Patent 7,252,986

Iliuta I, Larachi F (2005) Modeling simultaneous biological clogging and physical plugging in trickle-bed bioreactors for wastewater treatment. Chem Eng Sci 60(5):1477–1489

Jackson JV, Edwards VH (1972) Kinetics of substrate inhibition of exponential yeast growth. Biotechnol Bioeng 17: 943–964

Jia Y, Aagaard P, Breedveld GD (2007) Sorption of triazoles to soil and iron minerals. Chemosphere 67:250–258

Johnson R, Pankow J, Bender D, Price C, Zogorski J (2000) Environ Sci Eng 2–9

Khan FI, Husain T (2003) Evaluation of a petroleum hydrocarbon contaminated site for natural attenuation using 'RBMNA' methodology. Environ Model Softw 18(2): 179–194

Kim H, Peter RJ, Young LY (2004) Simulating biodegradation of toluene in sand column experiments at the macroscopic and pore-level scale for aerobic and denitrifying conditions. Adv Water Resour 27(4):335–348

Koussis AD, Pesmajogloua S, Syriopoulou D (2003) Modelling biodegradation of hydrocarbons in aquifers: when is the use of the instantaneous reaction approximation justified? J Contam Hydrol 60(3–4):287–305

Lai B, Shieh K (1997) Substrate inhibition kinetics in a fluidized bioparticle. Chem Eng J 65:117–121

Långmark J, Storeya MV, Ashboltb NJ, Stenström TA (2004) Artificial groundwater treatment: biofilm activity and organic carbon removal performance. Water Res 38(3): 740–748

Liang C, Chiang P (2007) Mathematical model of the non-steady-state adsorption and biodegradation capacities of BAC filters. J Hazard Mater 139(2):316–322

Liang C, Chiang P, Chang E (2007) Modeling the behaviors of adsorption and biodegradation in biological activated carbon filters. Water Res 41(15):3241–3250

López-Fiuza J, Buys B, Mosquera-Corral A, Omil F, Méndez R (2002) Toxic effects exerted on methanogenic, nitrifying and denitrifying bacteria by chemicals used in a milk analysis laboratory. Enzyme Microb Technol 31:976–985

Luong JHJ (1987) Generalization of Monod kinetics for analysis of growth data with substrate inhibition. Biotechnol Bioeng 29:242–248

MacQuarrie KTB, Sudicky EA, Frind EO (1990) Simulation of biodegradable organic contaminants in groundwater: 1. Numerical formulation in principal directions. Water Resour Res 26(2):207–222

Mayer KU, Benner SG, Frind EO, Thornton SF, Lerner DN (2001) Reactive transport modeling of processes controlling the distribution and natural attenuation of phenolic compounds in a deep sandstone aquifer. J Contam Hydrol 52(3–4):341–368

McCuen RH, Surbeck CQ (2008) An alternative to specious linearization of environmental models. Water Res 42(15):4033–4040

McNab WW, Dooher BP, Rice DW, Kavanaugh MC, Johnson PC, Cullen SJ, Everett LG, Kastenberg WE (1997) Assessment of appropriate fuel hydrocarbon risk management strategies for George Air Force Base, Victorville, California using a risk based approach. Lawrence Livermore National Laboratory, University of California. UCRL-AR-125619

Mohamed M, Hatfield K (2005) Modeling microbial-mediated reduction using the quasi-steady-state approximation. Chemosphere 59:1207–1217

Mohamed M, Hatfield K, Hassan AE (2006) Monte Carlo evaluation of microbial-mediated contaminant reactions in heterogeneous aquifers. Adv Water Resour 29: 1123–1139

Mohamed M, Hatfield K, Perminova IV (2007) Evaluation of Monod kinetic parameters in the subsurface using moment analysis: theory and numerical testing. Adv Water Resour 30:2034–2050

Mohamed M, Saleh N, Sherif M (2010a) Modeling in-situ benzene bioremediation in the contaminated Liwa Aquifer (UAE) using the slow-release oxygen source technique. Environ Earth Sci 61(7):1385–1399

Mohamed M, Hatfield K, Hassan AE, Klammler H (2010b) Stochastic evaluation of subsurface contaminant discharges under physical, chemical, and biological heterogeneities. Adv Water Resour 33(7):801–812

Mohamed M, Saleh N, Sherif M (2010c) Sensitivity of natural attenuation to variations in kinetic and transport parameters. Bull Environ Contam Toxicol 84(4):443–449

Molz FJ, Widdowson MA, Benefield LD (1986) Simulation of microbial growth dynamics coupled to nutrient and oxygen transport in porous media. Water Resour Res 22(8):1207–1216

Monod J (1949) The growth of bacterial cultures. Annu Rev Microbiol 3:371–394

Murphy EM, Ginn TR (2000) Modeling microbial processes in porous media. Hydrogeol J 8:142–158

Murphy EM, Ginn TR, Chilakapati A, Resch CT, Phillips JL, Wietsma TW, Spadoni CM (1997) The influence of physical heterogeneity on microbial degradation and distribution in porous media. Water Resour Res 33(5):1087–1103

Muslu Y (2000) A study on performance characterization of suspended growth systems. Water Air Soil Pollut 124: 285–300

Odencrantz JE, Valocchi AJ, Rittmann BE (1990) Modeling two-dimensional solute transport with different biodegradation kinetics. In: Proceedings of the petroleum hydrocarbons and organic chemicals in groundwater: prevention, detection and restoration, National Water Well Association, Houston, TX, pp 355–368

Ohtake H, Fuji E, Toda K (1990) Bacterial reduction of hexavalent chromium: kinetic aspects of chromate reduction by *Enterobacter cloacae* HO1. Biocatalysis 4(2):227

Papagianni M, Boonpooh Y, Matty M, Kristiansen B (2007) Substrate inhibition kinetics of *Saccharomyces cerevisiae* in fed-batch cultures operated at constant glucose and maltose concentrations levels. J Ind Microbiol Biotechnol 34:301–309

Phanikumar MS, Hyndman DW (2003) Interactions between sorption and biodegradation: exploring bioavailability and pulsed nutrient injection efficiency. Water Resour Res 39(5):1122. doi:10.1029/2002WR001761

Phanikumar MS, Hyndman DW, Wiggert DC, Dybas MJ, Witt ME, Criddle CS (2002) Simulation of microbial transport and carbon tetrachloride biodegradation in intermittently fed aquifer columns. Water Resour Res 38(4):1033. doi: 10.1029/2001WR000289

Phanikumar MS, Hyndman DW, Zhao X, Dybas MJ (2005) A three-dimensional model of microbial transport and

biodegradation at the Schoolcraft, Michigan, site. Water Resour Res 41:5011. doi:10.1029/2004WR003376

Prommer H, Barry DA, Davis GB (1998) A one-dimensional reactive multi-component transport model for biodegradation of petroleum hydrocarbons in groundwater. Environ Model Softw 14(2–3):213–223

Prommer H, Barry DA, Davis GB (2002) Modelling of physical and reactive processes during biodegradation of a hydrocarbon plume under transient groundwater flow conditions. J Contam Hydrol 59(1–2):113–131

Rashid M, Kaluarachchi J (1999) A simplified numerical algorithm for oxygen- and nitrate-based biodegradation of hydrocarbons using Monod expressions. J Contam Hydrol 40(1):53–77

Ribes J, Keesman K, Spanjers H (2004) Modeling anaerobic biomass growth kinetics with a substrate threshold concentration. Water Res 38(20):4502–4510

Rifai HS, Bedient PB (1990) Comparison of biodegradation kinetics with an instantaneous reaction model for groundwater. Water Resour Res 26:637–645

Rittmann BE, McCarty PL, Roberts PV (1980) Trace-organics biodegradation in aquifer recharge. Ground Water 18: 236–243

Saiers JE, Guha H, Jardine PM, Brooks S (2000) Development and evaluation of a mathematical model for the transport and oxidation–reduction of CoEDTA. Water Resour Res 36:3151–3165

Salvage KM, Yeh GT (1997) Development and application of a numerical model of kinetics and equilibrium microbiological and geochemical reactions (BIOKEMOD). J Hydrol 209:27–52

Schafer W (2001) Predicting natural attenuation of xylene in groundwater using a numerical model. J Contam Hydrol 52:57–83

Schirmer M, Butler BJ, Roy JW, Frind EO, Barker (1999) A relative-least-squares technique to determine unique Monod kinetic parameters of BTEX compounds using batch experiments. J Contam Hydrol 37:69–86

Schirmer M, Molson JW, Frind EO, Barker JF (2000) Biodegradation modeling of a dissolved gasoline plume applying independent laboratory and field parameters. J Contam Hydrol 46(3–4):339–374

Semprini L, Hopkins GD, Roberts PV, Grbic-Galic D, McCarty PL (1991) A field evaluation of in-situ biodegradation of chlorinated ethenes: Part 3. Studies of competitive inhibition. Gr Water 29:239–250

Sheintuch M, Tartakovsky B, Narkis N, Rebhun M (1995) Substrate inhibition and multiple states in a continuous nitrification process. Water Res 29:953–963

Shen H, Wang YT (1994) Modeling hexavalent chromium reduction in *E. coli* 33456. Biotechnol Bioeng 43(4):293

Simkins S, Alexander M (1984) Models for mineralization kinetics with the variables of substrate concentration and population density. Appl Environ Microbiol 47:1299–1306

Simpson DR (2008) Biofilm processes in biologically active carbon water purification. Water Res 42(13):2839–2848

Sims JL, Sims RC, Matthews JE (1989) Bioremediation of contaminated surface soils. R.S. Kerr Environmental Research Laboratory, U.S. Environmental Protection Agency, Ada, UK

Smith LH, McCarty PL (1997) Laboratory evaluation of a twostage treatment system for TCE cometabolism by a methaneoxidizing mixed culture. Biotechnol Bioeng 55:650–659

Strigula N, Detteb H, Melasc VB (2009) A practical guide for optimal designs of experiments in the Monod model. Environ Model Softw 24(9):1019–1026

Surmacz-Gorska J, Gernaey K, Demuynck C, Vanrollehem P, Verstraete W (1996) Nitrification monitoring in activated sludge by oxygen uptake rate (OUR) measurements. Water Res 30:1228–1236

Tanyola A, Tuncel SA (1993) Effectiveness factor for spherically growing mixed culture in substrate inhibition media. Enzyme Microb Technol 15:144–149

Tebes-Stevens CL, Valocchi AJ (2000) Calculation of reaction parameter sensitivity coefficients in multicomponent subsurface transport models. Adv Water Resour 23(6): 591–611

Tomson AFB, Jackson KJ (2000) Reactive transport in heterogeneous systems: an overview. In: Lichtner P et al (eds) Reactive transport in porous media, vol 36. Mineralogical Society of America, Washington, DC, pp 269–310

Vainshtein M, Kuschk P, Mattusch J, Vatsourina A, Wiessner A (2003) Model experiments on the microbial removal of chromium from contaminated groundwater. Water Res 37(6):1401–1405

Vavilin VA, Lokshina LY (1996) Modeling of volatile fatty acids degradation kinetics and evaluation of microorganism activity. Bioresour Technol 57:69–80

Vesper SJ, Murdoch LC, Hayes S, Davis-Hooverb WJ (1994) Solid oxygen source for bioremediation in subsurface soils. J Hazard Mater 36:265–274

Wang Y, Shen H (1997) Modeling Cr(VI) reduction by pure bacterial cultures. Water Resour Res 31(4):727–732

Watson JE, Gardner WR (1986) A mechanistic model of bacterial colony growth response to substrate supply. A paper presented at the Chapman conference on microbial processes in the transport, fate, and in situ treatment of subsurface contaminants, Snowbird, UT

Weaver JW, Charbeneau RJ (2000) A screening approach to simulation of aquifer contamination by fuel hydrocarbons (BTEX and MTBE). National Exposure Research Laboratory, United States Environmental Protection Agency, Athens, Georgia, pp 1–47

Woodward D (1996) Potential for contamination of the Liwa aquifer by disposal of Brine in the Bu Hassa and Asab Fields, Abu Dhabi

Yamamoto K, Kato J, Yano T, Ohtake H (1993) Kinetics and modeling of hexavalent chromium reduction in *Enterobacter cloacae*. Biotechnol Bioeng 41(1):129

Yoshida H, Yamamoto K, Yogo S, Murakami Y (2006) An analogue of matrix diffusion enhanced by biogenic redox reaction in fractured sedimentary rock. J Geochem Explor 90(1–2):134–142

Yu J, Molstad L, Frostegård Å, Aagaard P, Breedveld GD, Bakken LR (2007) Kinetics of microbial growth and degradation of organic substrates in subsoil as affected by an inhibitor, benzotriazole: model based analyses of experimental results. Soil Biol Biochem 39(7):1597–1608